Journal of Biomechanics ∎ (∎∎∎∎) ∎∎∎–∎∎∎

Contents lists available at ScienceDirect

Journal of Biomechanics

journal homepage: www.elsevier.com/locate/jbiomech
www.JBiomech.com

Understanding the fluid mechanics behind transverse wall shear stress

Yumnah Mohamied [a,b], Spencer J. Sherwin [a], Peter D. Weinberg [b,*]

[a] Department of Aeronautics, Imperial College London, United Kingdom
[b] Department of Bioengineering, Imperial College London, United Kingdom

ARTICLE INFO

Article history:
Accepted 5 November 2016

Keywords:
Hemodynamics
Wall shear stress
Atherosclerosis
TransWSS
Planarity
Pulsatility

ABSTRACT

The patchy distribution of atherosclerosis within arteries is widely attributed to local variation in haemodynamic wall shear stress (WSS). A recently-introduced metric, the transverse wall shear stress (transWSS), which is the average over the cardiac cycle of WSS components perpendicular to the temporal mean WSS vector, correlates particularly well with the pattern of lesions around aortic branch ostia. Here we use numerical methods to investigate the nature of the arterial flows captured by transWSS and the sensitivity of transWSS to inflow waveform and aortic geometry. TransWSS developed chiefly in the acceleration, peak systolic and deceleration phases of the cardiac cycle; the reverse flow phase was too short, and WSS in diastole was too low, for these periods to have a significant influence. Most of the spatial variation in transWSS arose from variation in the angle by which instantaneous WSS vectors deviated from the mean WSS vector rather than from variation in the magnitude of the vectors. The pattern of transWSS was insensitive to inflow waveform; only unphysiologically high Womersley numbers produced substantial changes. However, transWSS was sensitive to changes in geometry. The curvature of the arch and proximal descending aorta were responsible for the principal features, the non-planar nature of the aorta produced asymmetries in the location and position of streaks of high transWSS, and taper determined the persistence of the streaks down the aorta. These results reflect the importance of the fluctuating strength of Dean vortices in generating transWSS.

1. Introduction

The non-uniform distribution of atherosclerosis within arteries is widely attributed to influences of haemodynamic wall shear stress (WSS). The low, oscillatory WSS theory (Caro et al., 1971; Ku et al., 1985) underlies most current investigations of lesion localisation but not all studies have supported it (Peiffer et al., 2013b). Mohamied et al. (2015) showed that the multidirectionality of WSS during the cardiac cycle, characterised by the transverse wall shear stress (transWSS) metric (Peiffer et al., 2013a), may be a more significant factor. Subsequent studies have shown that high transWSS is collocated with atherosclerotic plaque prevalence in minipigs (Pedrigi et al., 2015), and is associated with transitional flow instabilities in regions prone to wall remodeling (Bozzetto et al., 2015; Ene-Iordache et al., 2015). There is increasing interest in multidirectional near-wall flow, with alternative indices being proposed (Arzani and Shadden, 2016; Morbiducci et al., 2015; Gallo et al., 2016).

TransWSS is the average over the cardiac cycle of WSS components perpendicular to the temporal mean WSS vector, with which endothelial cells are assumed to align (Chien, 2007). This provides the biological hypothesis that endothelial cells may be adversely affected by cross-flow, and indeed direct *in vitro* evidence supports this view (Wang et al., 2013). High transWSS may arise from large fluctuations of a small shear vector, small fluctuations of a large shear vector, or small fluctuations of a modest shear vector over a larger portion of the cardiac cycle, to name but three examples. The nature of the arterial flows captured by transWSS and the sensitivity of transWSS to waveform and geometry are not understood. This study uses numerical methods to investigate the origins of transWSS in rabbit aortic geometries, in simplified versions of such geometries, and with modified inflow and outflow conditions. It focuses on large-scale features; flows around branch ostia will be considered in a later paper.

2. Methods

2.1. Geometries

Most simulations used geometries of immature rabbit thoracic aortas reconstructed from micro-CT scans of vascular corrosion casts (Peiffer et al., 2012).

* Correspondence to: Department of Bioengineering, Imperial College London, South Kensington Campus, London SW7 2AZ, UK.
E-mail address: p.weinberg@imperial.ac.uk (P.D. Weinberg).

http://dx.doi.org/10.1016/j.jbiomech.2016.11.035
0021-9290/

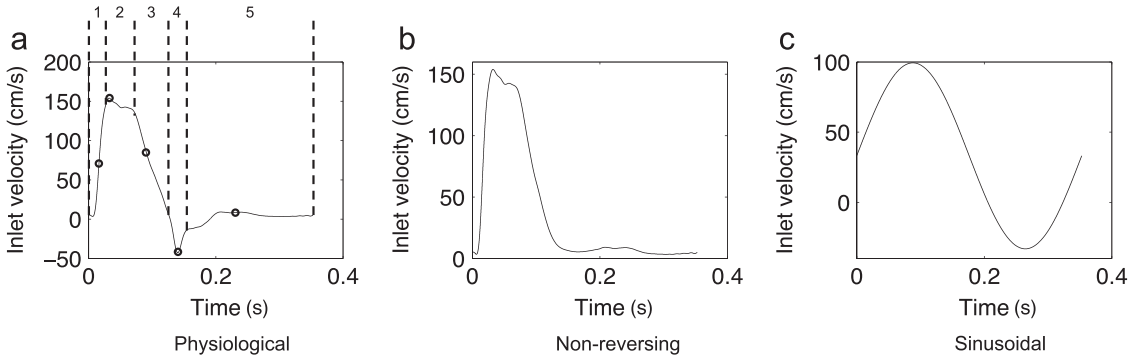

Fig. 1. Aortic flow waveforms applied at the aortic root (inlet), and at branch outlets in cases where branch flow was modeled. Five phases of the cycle that were investigated further are delineated by dotted lines (a); the five time-points (numbered) chosen to represent each phase are indicated by the circles on the waveform.

Two idealised geometries, both lacking taper and branches, were constructed from the centerline of one of these realistic geometries using SolidWorks: torsion and curvature were preserved in one ("non-planar" case) and only curvature in the second ("planar" case). The centerline was obtained using VMTK (Antiga et al., 2003). Curvature, κ, is the deviation of the centerline from a straight line and torsion, τ, is the twisting of the plane of curvature; both were computed using MATLAB 2014a. For the curve $\mathbf{r}(s)$, parametrised by the curvilinear abscissa s:

$$\kappa(s) = \frac{|\mathbf{r}'(s) \times \mathbf{r}''(s)|}{|\mathbf{r}'(s)|^3},$$

$$\tau(s) = \frac{[\mathbf{r}'(s) \times \mathbf{r}''(s)] \cdot \mathbf{r}'''(s)}{|\mathbf{r}'(s) \times \mathbf{r}''(s)|^2}.$$

The Frenet–Serret formulae, which define the three unit vectors for the Frenet frame (tangent **T**, normal **N**, and binormal **B**), are:

$$d\mathbf{T}/ds = \kappa\mathbf{N},$$

$$d\mathbf{N}/ds = -\kappa\mathbf{T} + \tau\mathbf{B},$$

$$d\mathbf{B}/ds = -\tau\mathbf{N}.$$

These, together with the definition of the tangent, $\mathbf{T} = d\mathbf{r}/ds$, allow a system of linear first-order differential equations to be solved for $\tau = 0$, which gives the centerline curve for the planar geometry.

2.2. Computational fluid dynamics

Time-dependent simulations were carried out on ~300 cores using the spectral/*hp* element framework Nektar++ (Karniadakis and Sherwin, 2013; Cantwell et al., 2015); two cycles were sufficient to dissipate initial transients. Rigid walls and Newtonian rheology were assumed with blood density $\rho = 1044\ \mathrm{kg\ m^{-3}}$ (Kenner et al., 1977) and dynamic viscosity $\mu = 4.043\ \mathrm{g\ m^{-1}\ s^{-1}}$ (Windberger et al., 2003). Tetrahedral element meshes with a 0.02*D*-thick prismatic element boundary layer (where *D* is the aortic root diameter) were generated with STAR-CCM+ using curvature-based surface triangulation. Minimum and average element sizes were approximately 0.007*D* and 0.25*D*, respectively, giving ~150,000 elements. Meshes equivalent to approximately 50 M linear tetrahedral elements were obtained by using fifth-order polynomial expansions. Mesh convergence and *p*-convergence tests were carried out; spatially averaged WSS at peak systole differed by 0.01% using polynomial orders 3 and 5, and by 1% using meshes of 140,000 and 200,000 elements.

A blunt inflow velocity profile was assumed at the aortic root and parabolic profiles at each branch outlet. These were initially modulated with a waveform (Fig. 1a) computed for the proximal descending aorta from a 1-D pulse wave propagation model (Alastruey et al., 2009). Further simulations were carried out with the reverse flow portion of the waveform removed (Fig. 1b) and with a sinusoidal waveform (Fig. 1c). A spatially- and temporally-averaged inflow Reynolds number of 300 was assumed.

Flow splits to the arch branches were based on experimental measurements (Barakat et al., 1997) with 14.7% to the brachiocephalic trunk and 7.1% to the left subclavian artery, and 2% of the descending aortic flow to the ten intercostal arteries (see Mohamied et al., 2015). Murray's law (Murray, 1926) was used for further flow divisions to individual branches. A no-slip condition was prescribed at the wall. A zero-velocity gradient boundary condition was imposed at the outlet, with a 0.75*D*-thick absorption layer (Israeli and Orszag, 1981) applied immediately upstream to damp out any instability introduced during the reverse flow portion of the cycle.

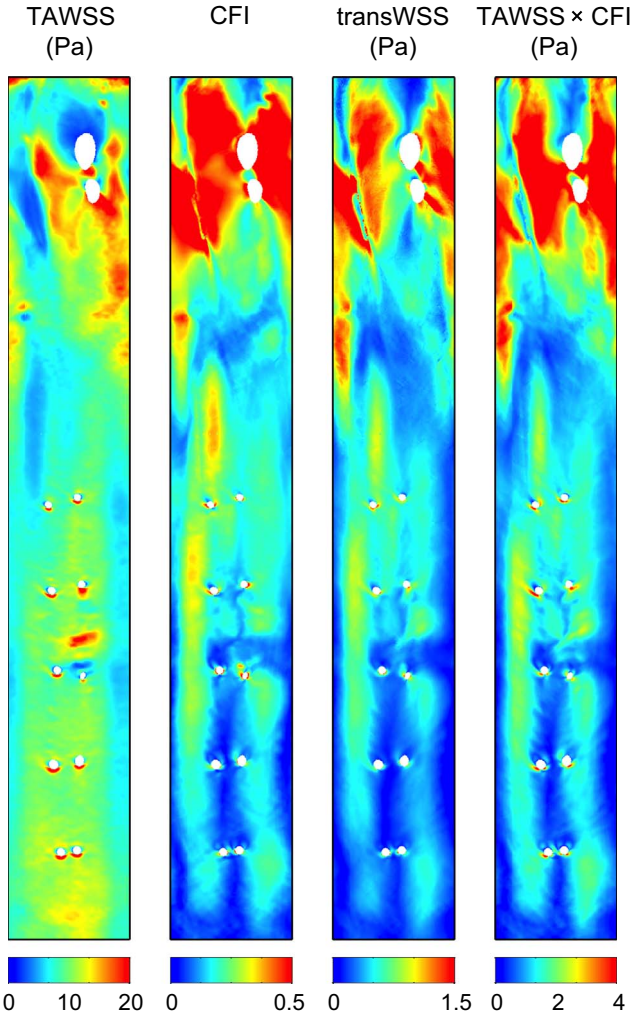

Fig. 2. Distributions of WSS metrics on the unwrapped luminal surface, viewed *en face*, for the anatomically and physiologically realistic simulation. TAWSS, transWSS and the product of time-averaged WSS and CFI are given in Pascals. Mean flow is from top to bottom, from the aortic root, over the arch (with two branch holes) and past the 5th intercostal pair. Anatomical left and right correspond to the right and left of each map, respectively. Note the different colour bars.

2.3. WSS parameters

Velocity gradients and consequent stress tensors were computed for all prismatic elements and projected on to the surface to obtain the WSS vector, $\boldsymbol{\tau}_w$. Time-

Please cite this article as: Mohamied, Y., et al., Understanding the fluid mechanics behind transverse wall shear stress. Journal of Biomechanics (2016), http://dx.doi.org/10.1016/j.jbiomech.2016.11.035